67-85:Template Journal 6/5/09 11:06 AM Page 309

Engineering application of thrust block analysis in slope stability problems in open pit mines

by K.N. Karparov* and M.F. Handley†

Synopsis

The classical limit equilibrium methods are suspected to be ineffective in predicting the potential for highwall failure in many instances in coal mines around the world. Slope engineers have for many years recognized a block thrust failure mechanism for slope failures, but little work had been done before 2000 to explain the actual mechanisms which must be responsible for the failure. The main reason for this is that limit equilibrium methods implicitly assume rigid blocks, and the resulting force equations must be satisfied everywhere simultaneously for them to have any meaning. This paper will show that the material involved in the slope failure is not rigid; indeed it undergoes considerable permanent deformation during failure. This observation allows the authors to treat the block boundaries independently, because they need not maintain a constant spatial relationship with one another, as is assumed in other methods. To enable analysis of this type the authors assume that the weight of the blocks is evenly distributed. This is reasonable, because the slope material is not strong enough to be self-supporting without some sort of constraint, or strong enough to be able to apply point loads to the surrounding material. The purpose of this paper is to extend the practical application of the analytical method developed from mechanism studies to provide an objective assessment of the risk of slope failure, and therefore guidelines for more stable slope designs. This work is based on studies carried out on two failures in an open pit coal mine in South Africa, and provides a methodology to assess the potential for failure more objectively than is possible with currently accepted methods, while at the same time remaining sufficiently simple to allow a 'back of the cigarette box' assessment by geotechnical engineers on site.

Introduction

Every rock or soil slope cut in open pit mining is susceptible to instability and eventual collapse. Open pit coal mines in South Africa are rarely deeper than 50–60 m, while examples of massive porphyry deposits such as Palaborwa and the copper-gold deposits in the Chilean Andes may be mined from pits deeper than 500 m. The pit sides in such instances are composed of a series of staggered highwalls or slopes stacked upon each other, much like a staircase, with the flat portions intervening between slopes known as benches. In many cases, each highwall or slope is vertical for economic and technical reasons. The overall pit slope angle is defined by a straight line that joins the crests of successive highwalls or slopes up the sides of the pit.

Highwall failure is an occurrence where rock or soil composing the highwall collapses, topples, slumps, or slides out. Not only is this dangerous, it forces a mine to perform some out-of-schedule clearing up, which can in some instances affect production plans, and therefore revenues, severely. Unlike other engineers, mining engineers cannot choose their materials, that is, they must design and cut their slopes in the rocks and soils that are present to access the mineral resource they wish to extract.

Economically, it is obvious that the slope angles must be as steep as possible in order to remove as little overlying soil and rock as possible, while at the same time the slope angles must be flat enough to reduce the possibility of failure to an acceptable minimum. Designing a pit slope in order to strike the correct balance between economics and safety in open pit mines is called pit slope engineering. The more general term rock slope engineering includes not only mining applications but also civil engineering applications, such as road cuttings in hillsides.

The factors that reduce pit slope stability, and therefore increase the probability of failure, are mining-induced, geological, and hydrological in origin. Most pit slopes are inhomogeneous structures comprising anisotropic layers of soil and rock characterized by different material properties. In addition to the variability of the properties of the natural materials, they are in various states of decomposition from weathering and

* *Agricultural Engineering Services, National Department of Agriculture.*

† *Department of Mining Engineering, University of Pretoria.*

© *The Southern African Institute of Mining and Metallurgy, 2009.* *SA ISSN 0038–223X/3.00 + 0.00. Paper received Oct. 2008; revised paper received Feb. 2008.*

Transaction Paper

67-85:Template Journal 6/5/09 11:06 AM Page 310

groundwater, and they are discontinuous because of jointing, bedding or layering, and other large-scale geological structures such as igneous intrusions, faults, and folds. These composite structures often present unpredictable behaviour, raising questions about internal processes that take place once the slope has been cut, and their effect on stresses and deformations within the slope. Changes in groundwater and weathering processes initiated by the slope cut can also play important roles in slope failure.

Hoek and Bray's book[1] on rock slope engineering is one of the most recognized in the field of rock slope design, and was first published 33 years ago. The means for predicting the potential and size of structurally controlled failures in rock slopes (wedge, plane shear, and step-wedge models) are also well developed in the CANMET Pit Slope Manual[2]. Some slope failures observed in South African and Australian coal fields[3], involve a layer of weak rock in the slope with thickness approximately ¼ of the slope height. The weak layer is commonly shale, and is usually exposed at the toe (foot) of the slope, and usually dips toward the pit. This failure mode is characterized by significant downward movement of the ground surface behind the slope crest, accompanied by the horizontal thrust of the rock in front of it out into the pit, see Figure 1. The horizontal thrust is usually facilitated by the weak layer dipping toward the pit. This failure mechanism is known as the block thrust mechanism. Similar slope failures to the block thrust mechanism have also been reported elsewhere[4–7].

Skempton and Hutchinson[8] defined three major classes of slope movement, namely falls, slides, and flows. They have defined a number of schemes of classification, but none can include the block thrust mechanism satisfactorily. Stead and Scoble[9] analysed 226 slope failures that took place in British coal mines, where they found that in about 66% of the failures, the sliding occurs along a single-, double- or multi-planar surface angled toward the pit (see Figure 2). Because of the chaotic nature of a rock slope failure, it is not easy to recognize the mechanism of failure except in the first six cases shown in Figure 2, which account for only 34% of the failures studied. The remaining 66% could easily have included block thrust failures of one sort or another.

There are many methods to assess the stability of a rock slope. All these methods can be classified into two groups[10]:

- Limit equilibrium methods
- Methods based on the upper and lower bound theorems of plasticity.

This paper considers only the former, namely limit equilibrium methods, but applies them to non-rigid bodies. Generally, limit equilibrium methods analyse the disturbing forces acting on an assumed rigid body defined by imaginary boundaries within a volume of rock or soil, and compares these with the constraining forces. The disturbing forces would cause the body to move, while the constraining forces will keep the body in place. In rock, disturbing forces are usually groundwater pressure, the weight of the body under consideration, and moments in the case of toppling failure.

The constraining forces are friction, rock strength, and stabilizing moments. In limiting equilibrium, the constraining forces are the maximum they can be, e.g. the rock is loaded to its full strength, and/or the frictional forces are fully mobilized. If the disturbing forces are exactly equal to the maximum possible constraining forces, the body or mass will be in equilibrium, but in this case, limiting equilibrium. Limit equilibrium methods therefore evaluate the maximum possible restraining forces, and then compare these with the disturbing forces—if the latter are computed to be larger, the analysis predicts slope failure. If the prediction is wrong, it could be because of initial assumptions, such as rock properties, block rigidity, or projected or inferred geological structure in the slope.

The limit equilibrium methods can be divided on two sub-groups: linear and non-linear methods, but the procedures are broadly similar in concept[11]. The linear methods of analysis, which are most amenable to hand calculation, are the two-dimensional slope analysis technique adopting undrained shear strength, the method of slices, and wedge failure. These methods are simple to use since there is a linear equation for the factor of safety; for this reason they are extremely useful in practice. The nonlinear limit equilibrium methods apply effective stress analysis of a slope, where the effective stress is to be determined around an assumed failure surface or set of failure surfaces inside the slope. In practice, this is also achievable by dividing the material composing the slope into a number of imaginary slices.

The block thrust mechanism is also a limit equilibrium technique, but is more complex than the toppling, sliding, or collapse mechanisms already mentioned. In this case, a wedge-like block with the sharp end down forms in the rock

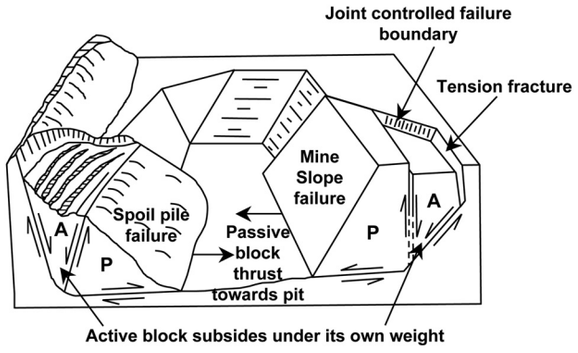

Figure 1—Slope and spoil failures reported by Boyd[7]

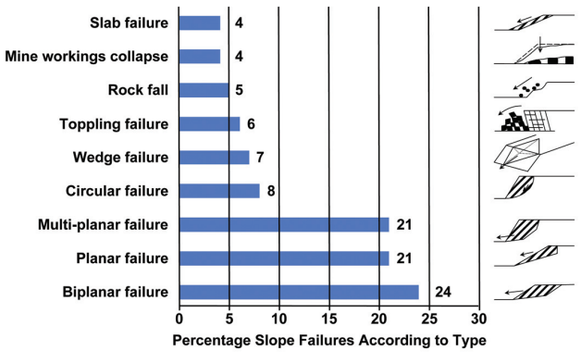

Figure 2—Typical failure modes, given in percentages, based on 226 study cases in coal mines in the United Kingdom (after Stead and Scoble[9])

67-85:Template Journal 6/5/09 11:06 AM Page 311

mass behind the highwall, by fracture processes that occur as a result of gravity loading and horizontal stresses present in the highwall. The wedge, by its formation, forms a second separate block of rock between the highwall side of the wedge, and the highwall face itself. If the wedge then thrusts downwards under its own weight, it thrusts the second block outwards (i.e. the highwall face) into the pit (see Figure 1). This mechanism is possible only if both blocks are deformable.

Wright *et al.*[12] undertook a survey in which they listed the characteristics of all accepted limit equilibrium methods, including the ordinary method of slices[13], Bishop's Modified Method[14], force equilibrium methods[15], Janbu's procedure for slices[16], the Morgenstern and Price method[17], and Spencer's[18] method. There seems to be some consensus that the Morgenstern-Price[17] method is one of the most reliable of these methods. The slices in all these methods are assumed to be rigid, and the normal force acting on the base of any slice is determined by resolving forces normal to the base of the slice. To make the problem determinate, the assumption is made that the resultant of the interslice forces acting on any slice is parallel to its base.

Unfortunately, the assumptions about the interslice forces do not satisfy static conditions and this may lead to an underestimate of the factor of safety by as much as 60%[19,20]. Basically, the assumption made about side forces is the main factor that distinguishes one limit equilibrium method from another, and yet is itself an entirely artificial distinction[11]. Since all the methods involve simplifying assumptions for a complex geotechnical environment, the chances of obtaining the 'correct' value of factor of safety will be reduced[10]. These weak points make simple limit equilibrium methods inapplicable in the back analysis of the above observed slope failures.

This paper first reviews two slope failures in a South African coal mine, and then describes the geological setting and history in which the coal seams formed. The geological history provides a basis for estimating the expected stress state in the mine before mining, because stress measurement data are difficult and expensive to obtain, and are therefore very scarce. The paper then introduces the thrust failure analysis Technique as a new approach to slope stability prediction in mines, and applies it to the two failures reviewed earlier.

The thrust failure analysis technique takes geotechnical conditions into account, including the effects of groundwater, in a simple Newtonian analysis of deformable blocks, which have formed in the slope as a result of fracture formation within the slope. The second implicit assumption made in these analyses is that because the blocks are deformable, the forces they exert on their mutual boundaries will be uniform on each boundary segment, and independent of those on other boundary segments. This allows independent force calculations for each boundary segment, and hence independent factor of safety calculations for each segment, that can be weighted by the segment lengths to find an overall factor of safety for the slope. We conclude that the method appears to provide more credible results than any of the available slope stability methods currently in use, but further work into fracture growth in rock within the slope is indicated, because this will elucidate block formation mechanisms, enabling better failure predictions.

Slope failures in a South African colliery

Opencast colliery 'A' strip mines three coal seams with an average total thickness of approximately 16 m. Figure 3 presents the colliery stratigraphic column[21], while a mine plan (not reproduced here) shows that underground mining by a previous colliery had left pillars in the middle coal seam in some areas, the bottom coal seam in other areas, with the result that sometimes there were coal pillars superimposed upon one another in the lower and middle seams. These mined seams daylight in the strip mine, and could contribute to slope instability. The upper coal seam was never mined by the old underground colliery. Two slope failures took place during different seasons and in different pits but in both cases the strata dipped towards the pit, and in both cases, none of the coal seams had been mined previously. Both failures took place after the middle coal seam had been exposed in the pit floor, but before the coal had been mined.

The first case of slope failure took place in Pit A-1 on the contact between shale and the middle coal seam, both of which dipped at 10° to 12° towards the pit. The top coal seam in the area was very thin (about 1 m thick). The failure took place in two stages: the initial failure (involving only the sandy overburden) and the major collapse, which slipped along the bottom contact of the shale layer above the middle coal seam. The slope profiles[22] before and after failure appear in Figure 4. The initial failure was probably circular because applied limit equilibrium methods for circular failure yielded a factor of safety of 0.72 for the slope.

The major collapse followed the cleaning operations after the circular failure, when the slope profile had a flatter slope angle than it had prior to the circular failure (see Figure 4). None of the rigid-block limit equilibrium methods named above predicted failure in the slope after the minor circular failure had occurred. The major failure indicates a multi-planar or blocky type of failure, but an applied block-

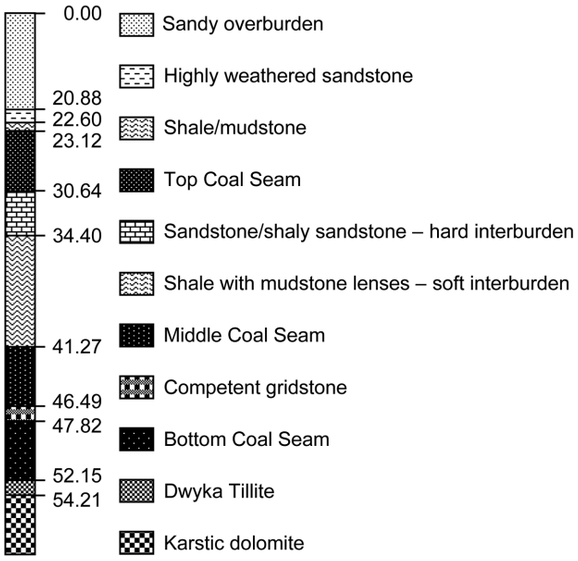

Figure 3—Representative stratigraphic column of the strip mine (after Mattushek[23])

67-85:Template Journal 6/5/09 11:06 AM Page 312

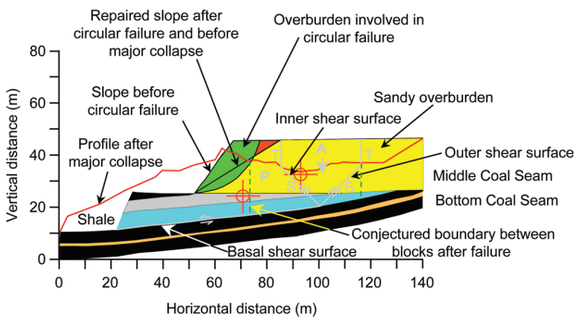

Figure 4—Slope profiles in Pit A-1 before and after circular failure, and after major collapse (after SRK[21])

specified technique used for the slope factor of safety calculation was not successful because it was higher than unity, indicating a stable slope. Mine plans from the old underground mine did not show any underground mining activities in the area underneath the failure, hence the two coal seams below the slope were intact.

Figure 4 shows the slope profile before the major failure, and the profile after failure in red. This is a clear indication that the theoretical blocks, marked in grey and labelled A and P for the active and passive blocks respectively, must have undergone deformation during failure. There must have been deformations in the slope before the failure, but these were not sufficiently noticeable to have warned mine personnel, because the failure was very unexpected. The volume of rock in the slope bulked from 1702 m^3 per m of slope to 2 444 m^3 per m of slope, indicating a bulking factor of 43.6% during failure. The conjectured boundary between the active and passive blocks after failure is given by assuming that both the active and passive blocks would bulk the same amount during failure, and then finding the boundary for the equivalent volume in the failed profile. It was also assumed that there was no mixing of the material from the two blocks during failure. The outer tensile boundary of the active block remains more or less in the same place after failure (shown by dark green dashed line to the right), if it is assumed that the active block bulks to the same degree as the passive block.

What is clear from Figure 4 is that the active block has lost gravitational potential energy, which would have provided the thrust of the passive block into the pit. The overall loss of gravitational potential energy for the whole slope is estimated by noting that the centre of gravity of the unfailed slope is 33 m above datum (right-hand red crossed circle in Figure 4), while the failed slope centre of gravity lies 24 m above datum (left-hand red crossed circle). Using the unfailed slope volume given above and assuming a unit weight of 25 kN/m^3, the potential energy change during failure is estimated at 383 MJ per m of slope.

If the whole slope moved 25 m to the left during failure (this is a crude estimate, because the centre of gravity of the failed slope is 25 m to the left, but the width of the failed material has increased, while its height has diminished), then energy consumption due to friction loss using a friction angle of 10° for the shale-middle coal seam contact is about 187 MJ per m of slope. This leaves nearly 200 MJ per m of slope for breaking the rock up and comminuting it. These calculations are rather crude estimates, but they indicate that a thrust mechanism is possible, at least from an energy balance calculation.

The second slope failure took place in Pit A-2 of the same colliery. Figure 5 presents the slope profile[22] before and after the failure. Mine spoils in piles between 20 m and 25 m high had been dumped at a distance of approximately 20 m behind the slope crest. Any joints that might have been responsible for wedge failure were not observed in the area. Without any visible indications or warnings of impending failure, the slope collapsed, and this failure involved the spoils, overburden, top coal seam, and the interburden between the top coal seam and the middle coal seam. This failure also took place above unmined ground, after the middle coal seam was exposed in the pit bottom, but before it was mined.

After the cleaning operations, the failure surface, again on the contact between the shale and the middle coal seam, was clearly visible in the pit. At the site of this failure, the strata dipped at an average angle of 16° towards the pit. The estimated factor of safety for circular failure of this slope varied between 2.4 and 2.6 depending on the method of calculation (Fellenius' Ordinary Method[13], Bishop's Modified Method[14], Janbu's Procedure for Slices[16], Morgenstern-Price[17], and Spencer[18]). Clearly, this failure could not have taken place by a circular mechanism. Using the above methods to analyse a block-type of failure mechanism gave very low safety factor values (0.11 to 0.14 for the Morgenstern-Price[17] method). The other methods, such as the Janbu[16] and Bishop[14] indicated slightly higher safety factors around 0.15, which suggest that the slope would have collapsed immediately, even while it was being cut. Fellenius' Ordinary Method[13] yielded a factor of safety of 1.2, which could be considered to be the 'best' result, even though it did not predict failure.

Assessing this slope using the volume-energy approach above is not so simple, because there is an approximate 1 178 m^3 per m of slope missing, if we assume that the spoil pile retains a constant volume during the failure process. It could have become compacted during collapse, but this would not account for the discrepancy. It is not clear from communication with the mine[22] whether any spoil and sandy overburden had been removed or not before the failed slope profile was measured, and there is no evidence that the spoil piles became compacted during failure.

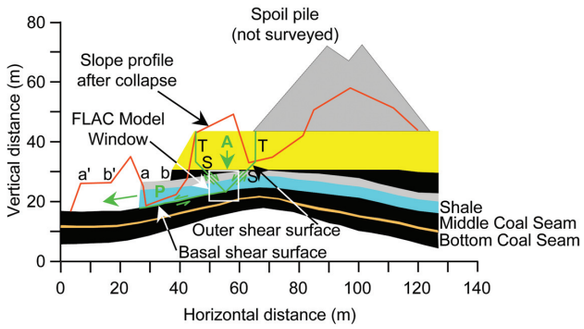

Figure 5—Slope profiles in Pit A-2 before and after major collapse (after Canady[22])

67-85:Template Journal 6/5/09 11:06 AM Page 313

The geometry of the failed slope strongly suggests a thrust mechanism, since points a and b are displaced 22 m into the pit to positions a' and b' (see Figure 5). The failed profile gives 704 m³ per m of slope as opposed to 625 m³ per m of unfailed slope, if the volume is computed while ignoring the spoil pile and the sandy overburden behind the constructed active block, see Figure 5. This accounts for a bulking factor of 13%, which is also credible if the individual blocks involved in the failure stayed more or less intact. Another factor that could account for the discrepancies found in the drawing could be the out-of-plane variation of the slope profile, and possible out-of-plane material movement. It is also not known whether the spoil pile profiles before failure were accurately represented or not.

The limit equilibrium methods fail because they assume rigid, homogeneous, and isotropic rock and soil without internal structure. Other failure mechanisms such as wedge failure or toppling failure listed by Stead and Scoble[9] and illustrated in Figure 2, were also not appropriate. Although the two failures were very different in character, it appears that both resulted from the same mechanism, since there were six features common to both:

- The slope fails by horizontal movement towards the pit by a front block (passive block) which can show varying degrees of disintegration
- The forward movement of the passive block is driven by the vertically downward movement of the active block behind, which ends up with a final elevation significantly lower than that of the original slope profile, and this block undergoes significant disintegration
- In both cases the slope is situated on strata dipping towards the pit
- In both cases the failure surface is on the contact between the shale and the middle coal seam
- The failure surfaces daylight at the toe of the unfailed slope in both cases
- Almost vertical tensile fractures were present on surface behind the slope crest, usually above the crest of the undulation in the coal-bearing strata.

The authors conclude that some sort of block thrust mechanism is responsible for both failures, even though the two originated in two very different slope geometries, and yielded very different results. In order to understand more clearly how the failures could have developed, it is necessary to review the geological history of the coal deposit, and the likely pre- and post-mining stress states in the mine slopes.

Geological history of the coal deposit

The coal deposit forms part of the Vaal Basin, which straddles the Gauteng-Orange Free State boundary in the area surrounding Vereeniging and Sasolburg. A representative stratigraphic column for Strip Mine A appears in Figure 3, which is reproduced after Mattushek[23], and shows the representative stratigraphic column in which slope failures occurred. The principal palæo-feature of the deposits is the uneven dolomite base, which has led to sediments deposited on it being uneven. The dolomite palæo-surface was formed in white dolomite belonging to the Transvaal Supergroup.

The coal-bearing strata above it are not uniformly thick or level, but undulate following the dolomite base. The coal seams, as well as the other strata, are thinner above palæo-highs and thicker above palæo-lows in the dolomite. This feature has resulted in strata dipping up to 15° between highs and lows on the dolomite palæo-surface. The dolomite highs themselves are dome-shaped and 200–300 m in diameter, giving them a hill-like form. Note that the undulated strata formations described are definitely not tectonic formations, but are the result of weathering and chemical erosion, which sculpted a karstic topography on the dolomitic basement[24].

The karst formation in the dolomite was followed by glaciation, which smoothed the rugged karstic topography and formed tillite deposits in the topographic lows. Cairncross[24] states that the lignite-bearing (later coal-bearing) sequence accumulated in the fringes of fluid-glacial currents at the end of the Paleozoic when the southern tip of Africa was located near the South Pole. The development of lignite on top of glacial deposits represents the corresponding rise in temperatures as Africa drifted northwards from extreme southern latitudes.

The lignites formed from vegetal matter being washed down into a lake. A gradually more temperate climate allowed the growth of mostly deciduous vegetation in a swampy near-shore environment where rivers transported re-worked glacial tillite materials and plant matter into a subsiding intracratonic basin. The lignite-bearing strata probably represent the gradual formation and final drowning of retrogressive deltaic lobes, where fluid-glacial features of the Dwyka formation are overlain by retrograde deltaic sediments, which are in turn overlain by beach and marine deposits of the now-recognized hard overburden and hard interburden as the sea level gradually rose[24] (see the stratigraphic column in Figure 3).

As mentioned earlier, the undulating strata reflect the underlying dolomitic palæo-surface by having a similar topography, in that they are approximately circular in plan with a diameter of a few hundred metres and have a hill-like form. Further widening and joining of the karstic features in the dolomite after the deposition of the overlying sediments also contributed to the degree of undulation in formations in the overlying strata. Diagenesis and coalification of the lignite deposits occurred after the onset of regional extension related to the break-up of Gondwana during the late Paleozoic to early Triassic, and the corresponding intrusion of doleritic dykes[25].

The geological history of the coal-bearing succession has an important bearing on shaping the pre-mining stress state, which in turn has an influence on slope behaviour during mining. Since the strata undulation was not tectonic, it simplified the modelling because the authors did not have to estimate a horizontal tectonic stress that would have been sufficient to cause the undulation in the strata, and thereafter make assumptions of what happened to the tectonic stress.

Inferred stress state in mine slopes

The Earth's crust and conditions therein remain almost completely unexplored, especially the stress state of the solid crust. This is because stress measurement in rock and soil is

67-85:Template Journal 6/5/09 11:06 AM Page 314

a notoriously difficult and expensive process, and therefore stress data remain rare (see for example Voight[26], Gay[27,28], Stacey and Wesseloo[29], and Sellers *et al.*[30]). Rock stress estimates are therefore usually based on fundamental theory, a small number of measurements, and a large amount of deduction and inference. In the case of the slope stability study, slope stress estimation was no different.

In the only references relevant to the coal mine in question, Van der Merwe[31,32] mentions that horizontal stress near the surface in coal mines is of the order of twice the vertical stress. The vertical stress in turn, must be equal to the overburden weight from equilibrium considerations. In the absence of any other convincing data, the authors assume that the horizontal stresses in the slope before it was excavated were of the order of twice the vertical stress for the following reasons:

- Van der Merwe's[31,32] comments
- Hoek and Brown[33] indicate that horizontal stresses are between one and three times larger than vertical stresses at shallow depth
- The undulations in the coal-bearing strata were the result of 'draping' the strata over a previously uneven terrain rather than folding due to horizontal compressive stresses.

From the above, the authors assumed a vertical stress equivalent to the overburden weight, and a directionally isotropic horizontal stress exactly double the vertical stress. In addition to the above, the authors assumed that the underground coal mine would not have resulted in significant changes to the original stress state before mining—this is confirmed by numerical modelling[34], but not shown here. Slope failure took place after the slope was cut; hence it was necessary to compute the stress state in the slope after it was cut. This was done using the two-dimensional finite difference scheme FLAC[35]. The FLAC (Fast Lagrangian Analysis of Continua) model developed contains the undulating geological structure described above, and also takes into account the anisotropic properties of the shale above the middle coal seam. The other strata in the model are each assumed to be isotropic, homogeneous, and intact, even though they do not all have the same mechanical properties[34]. The slope as a whole is therefore heterogeneous, because it consists of several layers, each with its own set of properties.

The mine slope models were developed using the pre-failure profiles shown in Figures 4 and 5 in order to estimate the stress in the slopes using FLAC35. The stress states estimated from the model are therefore a result of the undulating geologic structure, excluding the effect of discontinuities, tectonic history, and weathering, all of which cannot be taken into account in the model. The effects of groundwater will be detailed and dealt with in the thrust failure analysis later.

The results of the stress state after mining appear in Figure 6. Figure 6 is a 'zoom' into the model of the slope, so that the stress distribution can be seen more clearly. The 'zoom window' is shown by a white square in Figure 5, and it centres on conditions at the base of the wedge. The finite difference zones appear as green parallelograms, and the principal stress tensor in each zone is represented by a cross whose limb lengths are proportional to the magnitudes of the stress components, and whose directions represent the principal stress directions. The stress state at the base of the wedge in Figure 4 is not significantly different, and is not shown here. The stress state shown is that for a continuum and therefore represents the stress state that would have existed in the slope before the blocks had formed. The most important features of the stress distribution are:

- The formation of a tensile horizontal stress near the surface behind the slope (not shown, because a plot of the whole slope would be too cluttered to see any detail)
- The rotation of the stress tensor to lie parallel with the inclined strata
- The discontinuous change (at this level of approximation) in magnitude of the minor principal stress—parallel to the strata—between the shale and the sandstone
- The continuity of the stress tensor across the shale-coal contact
- The uniformity of the stress state in each stratum because of the rock material deformability.

These features are critical to the development of the failure model for the slope, and they support our assumption that the stresses on the block boundaries will be uniform, and independent of each other.

Block formation in mine slope

Unexpected slope failures occurred in two instances, in both of which it is probable that active and passive blocks were first formed by the growth of failure surfaces within the slope after it had been cut. These failure surfaces combined to form independent deformable blocks, which were sufficiently unstable to result in the collapse of the slope into the mine pit. Although underground mining had taken place on the middle and bottom coal seams before the strip mine commenced operations, neither of the slope collapses took place over mined ground. Therefore the effect of mined ground on slope stability will no longer be considered in this paper, but interested readers can consult Karparov[34] for further details.

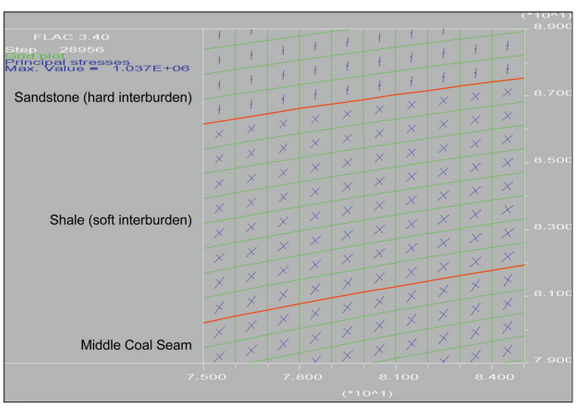

Figure 6—Principal stress distribution in slope before slope collapse

67-85:Template Journal 6/5/09 11:06 AM Page 315

Vertical fractures

Vertical tensile fractures commonly develop in the ground behind a mine slope crest, and the coal mine in question was no exception. The stress modelling confirms that tensile cracks should develop, as shown in Figure 7, which presents a plot of the horizontal stress component along a vertical profile line above the crest of the undulating formation. There is a significant increase in the tensile stress component together with an increase in depth of the tensile zone when a slope has been cut. The significance of these results is that conditions conducive to surface tensile cracking are generated by a combination of mining and the subsurface geological structure.

In a series of very detailed model studies on slope failures, Barton[36] found that the tension crack behind the slope crest was generated by small movements within the rock mass, and that it appeared after slope excavation. Although these individual movements were very small, their cumulative effect was a significant displacement of the slope surface—sufficient to cause separation of material behind the slope crest and to form tension cracks. The vertical active block boundaries are defined by vertical tensile cracks. We therefore assume the existence of these fractures before failure, because they are favoured in the model, and have been observed in the coal mine in question, both at the slope failures, and elsewhere.

Failure surface on shale–middle coal seam contact

Failure in rock is still poorly understood because of the variety and complexity of processes that lead to it. State-of-the-art finite difference schemes such as FLAC[35] are not able to produce credible failure results for rock because the rock mass material in the model is assumed to be continuous, even if heterogeneity and anisotropy have been taken into account. The modelled rock material remains continuous throughout, even after modelled failure. In contrast, rock material in reality would shear and fracture, thereby becoming more discontinuous during the process of failure. Hence model results diverge from reality once the material starts to break up. Since the models on their own are unable to confirm slope failure in the geotechnical conditions described above, investigation into the mechanisms through which failure can eventually result along the shale-middle coal seam contact are indicated, and are briefly discussed below.

Although it is not a central theme to the study, Karparov[34] investigated how a failure surface could develop on the shale-middle coal seam contact by recourse to the study of thin sections of the shale under the microscope, fracture mechanics theory, and the modelled stress state in the slope after mining, and before slope collapse. This work did not produce incontestable results, but it does point to possible mechanisms by which a failure surface could slowly develop along the shale-middle coal seam contact. This surface is clearly central to the slope collapse (see Figures 4 and 5), and because the collapsing rock mass slid on it, any delicate features that may have pointed to the mechanism of its formation have been obliterated. Even though the mechanism of its formation remains unconfirmed, this failure surface is accepted as being critical in the slope collapses, since it was found on the shale-middle coal seam contact in both cases.

Inclined shear surfaces to form block wedge and failure

The authors conjecture that sometime after the formation of the tensile fractures, shear fractures must have started developing in the slope to define the block wedge. Whether or not this took place before or after the formation of the failure surface on the shale-middle coal seam contact is debatable, and should form the subject of further research. Even in solid rock material (where jointing and other structures are insignificant), shear failure remains a complex process resulting in complex fracture structures[37–42]. A synthesized shear fracture containing all the features, and based on the work of Riedel[37], Vermeer and De Borst[40], and Ortlepp[41], appears in Figure 8. A photograph of a shear fracture in hard rock appears in Figure 9.

The purpose of presenting all this detail is to recognize that the formation of shear zones in the slope will be complex, just as they are in any geological material. Although the structure of a shear fracture zone is complex, its overall orientation is simple, i.e. it can be assumed to lie parallel with the direction of the maximum shear stress in the slope. Shear bands or fractures, however, need not occur at only one specific angle, but could occur over a range of angles in relation to the maximum principal stress direction

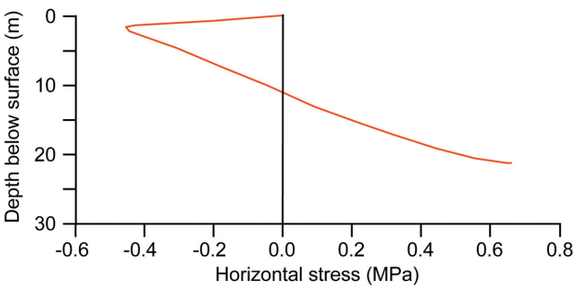

Figure 7—Horizontal stress in slope behind slope crest, on vertical line above formation crest

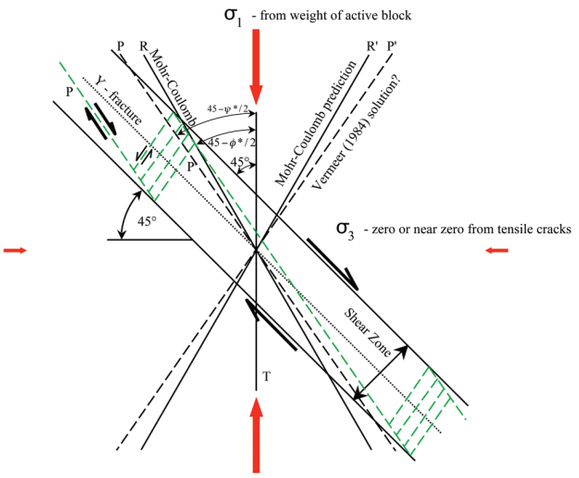

Figure 8—Riedel structures in brittle material (after Riedel[37])

67-85:Template Journal 6/5/09 11:06 AM Page 316

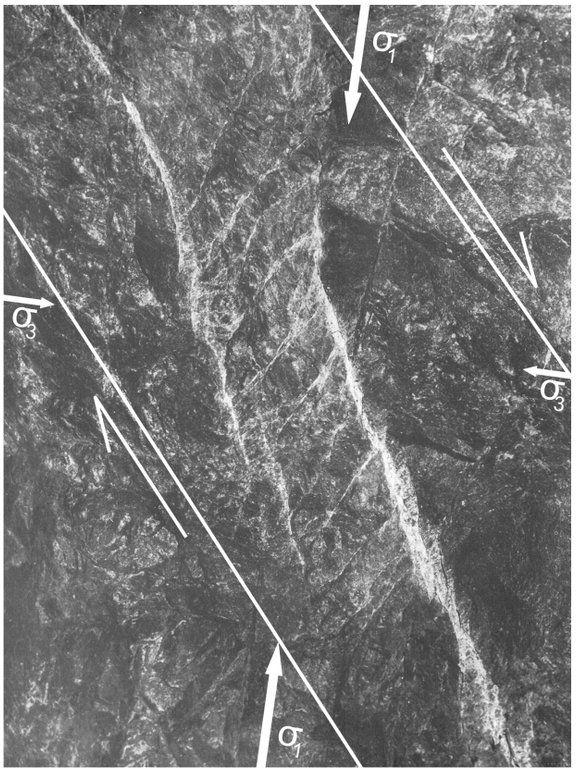

Figure 9—Example of a shear fracture in brittle rock in a deep level gold mine showing Riedel Structures (after Ortlepp[41])

together with the effects of anisotropy in the shale (e.g. Jaeger and Cook[43]). Note that only one possible Riedel Shear Structure is drawn in green in Figure 8, in which the conjectured Vermeer and De Borst[35] dilation solution has been applied. The other possible Mohr-Coulomb alternative is not shown for purposes of keeping the drawing clear.

With reference to the FLAC solution before block formation given in Figure 6, the authors conjecture that the shear zones are inclined at 45° to the horizontal, and that they are approximated by straight lines, although this need not be the case in reality. We conjecture that as the active block starts becoming separated from the surrounding rock mass by small movements. Shear fractures can now form at 45° to the horizontal. The authors deduce from the model, and information available that they are more likely to develop downwards from the bottom of the tensile fractures, since the stress state in the slope is more favourable for shear zone development at the base of the tensile cracks because the horizontal stresses there are effectively zero.

Constructing the active-passive block geometry for the above case studies

When the artificial cut is made, fracture propagation starts because of rock relaxation. At this time, the vertical tensile fractures develop at ground surface behind the slope crest, and the possible tensile fracture at the toe of the slope along the shale-middle coal seam contact surface forms for a short distance into the toe.

Karparov[34] presents a criterion for estimating the depth it penetrates, but further research will be necessary to confirm this. The shear zones develop at approximately 45° to the horizontal through the unbroken rock between the tensile fractures and the shale-middle coal seam contact. During the shear process to form the apex of the wedge, the rock in the shear zones will start to dilate (expand). This will generate a horizontal force on the passive block, which will accelerate the development of the purely frictional surface on the shale-middle coal seam contact.

At some point (probably before the two shear zones converge), the material between the shear zones will begin to crush under the weight of the overlying material comprising the active block. This will accelerate horizontal rock dilation, both in the shear zones and in the crushed rock at the base of the wedge. These dilationary forces may be sufficient to thrust the passive block into the pit, and as this happens the active block will continue to slump downwards under its own weight, forcing the passive block further out into the pit. The whole process ends when the active block ceases to slump downwards, thereby dissipating the dilationary forces that are driving the passive block into the pit. During this process both blocks become comminuted, and the active block perhaps more so than the passive block. Figures 10 to 17 give a sequence of events the authors have deduced must take place during the slope failure. Based on this mechanism, the conjectured active and passive blocks appear in Figures 4 and 5 for the two mine slope failures.

Once these fractures have formed, continued slope stability is seen to be only a consequence of the balance of forces existing between the blocks in the profile, and that this

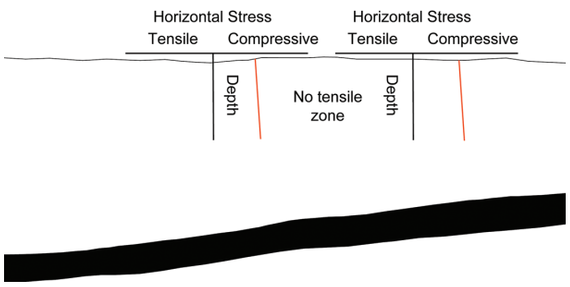

Figure 10—Middle Coal Seam before mining, with virgin horizontal stress profile

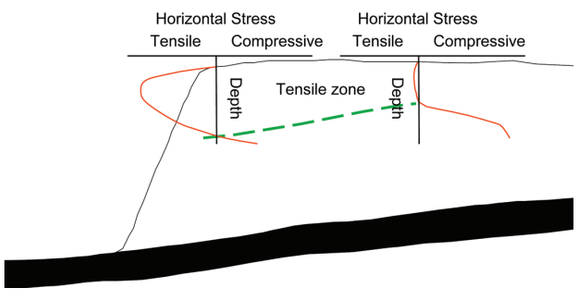

Figure 11—Slope cut to expose seam, with resultant horizontal stress profile

67-85:Template Journal 6/18/09 2:58 PM Page 317

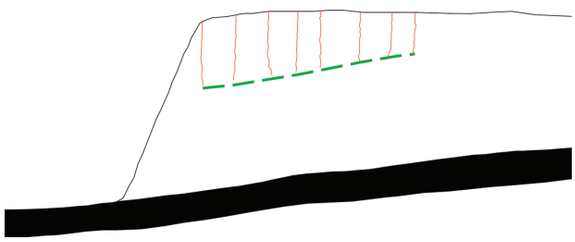

Figure 12—Development of tensile cracks behind slope crest

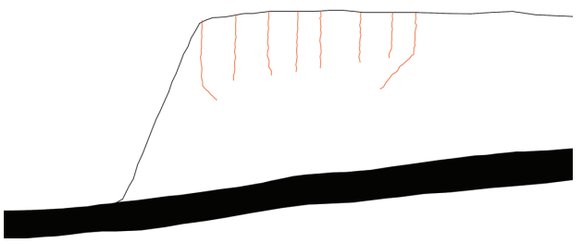

Figure 13—Commencement of shear fracture growth

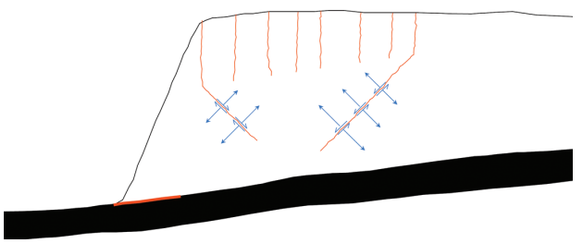

Figure 14—Continued shear fracture growth with attendant dilation, and degradation of any cohesion along top coal contact

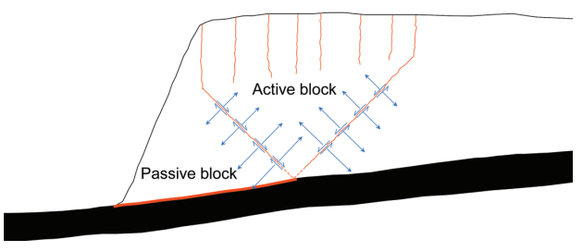

Figure 15—Active and passive blocks now fully defined by fracture growth in the slope

provides an important clue for a simple in-pit calculation that will be introduced later. It is important to recognize that this analysis considers only force equilibrium and assumes that all forces pass through the block centroids. In other words, moment equilibrium is not considered in this model because observations of the failures at the mine did not reveal any significant rotational motion in the failures.

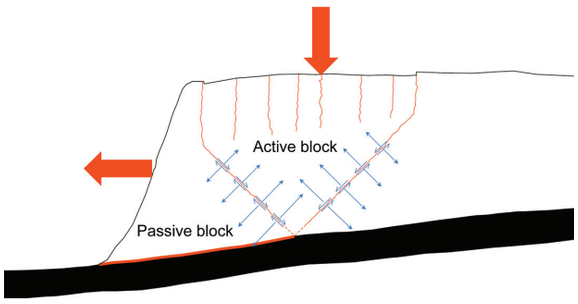

Figure 16—Minor slumping of active block behind slope crest as it continues to crush at the wedge tip below

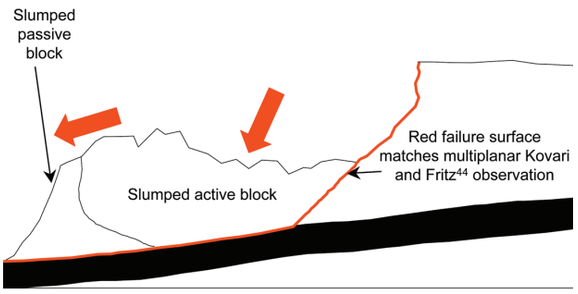

Figure 17—Final slope collapse leaving evidence of a bi-planar or multi-planar failure surface described by Stead and Scoble[9], and Kovari and Fritz[44]

Karparov[34] provides a very detailed account of how all the forces, including those derived from groundwater, are computed, and these appear in Appendix A. The computations are based on Newton's Laws of Motion, while the block stability is estimated assuming deformable active and passive blocks and a factor of safety approach to the potential of slip failure on the block sides and on the shale-middle coal seam contact in the observed failure cases discussed above. This methodology should not be confined to the cases discussed above only; it can be adapted to the geotechnical conditions in any open pit.

Since the blocks are deformable, the authors assume that the stresses along the block boundaries are approximately constant, and independent of each other. This makes it possible to calculate factors of safety for each boundary, and then finding a weighted average using the lengths of the respective fracture surfaces that define the active block and passive blocks. The details are too lengthly to include here, all the information necessary to perform the analysis as it was described in Karparov[34] appears in Appendix A following this paper. Only the resultant formulæ necessary for the factor of safety calculations are presented below.

The inner surface factor of safety for failure is given by (see Appendix A for definition of variables and all the calculations necessary to compute the FoS):

$$FoS_i = \frac{\bar{c}_i l_i - U_i \tan\left(\bar{\phi}_i\right)}{\frac{P_A\left(1+\sin\omega_A\right)\sin\beta_i}{2} - R_P \sin\left(\bar{\phi}_i\right)}$$

67-85:Template Journal 6/5/09 11:06 AM Page 318

The outer surface factor of safety is given by:

$$FoS_o = \frac{\bar{c}_o l_o + \begin{bmatrix} P_A(1-\sin\omega_A)\cos\beta_o \\ 2 \\ -U_o - V_{CD}\sin\beta_o \end{bmatrix} \tan(\bar{\phi}_0)}{\bar{R} + \frac{P_A(1+\sin\omega_A)\sin\beta_o}{2} + V_{CD}\cos\beta_o}$$

The safety factor for the basal surface (shale-middle coal seam contact) is:

$$FoS_b = \frac{\begin{matrix} P_f \cos\omega_F \tan\phi_b + \\ (c_b l_C + P_C \cos\omega_C \tan\phi_b) - \end{matrix} (U_C + U_F)\tan\phi_b}{P_F \sin\omega_F + P_C \sin\omega_C}$$

Finally, the factor of safety combined as a weighted average for the slope is given by:

$$FoS = \frac{FoS_i l_i + FoS_o l_o + FoS_b l_b}{l_i + l_o + l_b}$$

The authors called the failure mechanism the thrust failure mechanism, because slope collapse occurs when the active block subsides under its own weight, thrusting the passive block into the pit. The mechanism is illustrated in Figure 1, while the contrast between the unfailed slope profile and failed slope profile shown in Figures 4, and 5 strongly suggest the mechanism.

The ultimate objective of Karparov's[34] thesis was to provide a simple calculation that could be used in pit to assess the stability of slopes such as those described above. This never materialized because of the geotechnical complexity at the two failure sites, and the complexity of the conjectured failure mechanism. The second author has considered possibilities of simplifying the required calculations sufficiently to make in-pit assessments possible, but these are probably fraught with error and inaccuracy because of the assumptions that have to be made. The following section gives a brief description of such a method, but this must be widely tested and shown to be reliable before it can be used with confidence.

Quick collapse potential calculation in pit using the block thrust model

The first part of this section contains a simple field calculation that can be performed from measurements of tensile fracture positions behind the slope crest, knowing the slope height, and the overall slope angle. This very simple guideline can be refined only by widespread testing. The second part of this section discusses the results of the detailed computations as they are outlined in Appendix A.

Simple criterion for FOS estimation whilst in the pit

Based on the above conjectures and assumptions, it is possible to sketch an approximate picture of the block formation and the subsequent slope failure. For this simple in-pit criterion calculation, general conditions are assumed as follows:

- The pit bottom is formed on a horizontal discontinuity that daylights at the toe of the slope
- Fracture toughness and rock strength are ignored, and therefore the active and passive blocks are assumed to have formed
- All the natural as well as the block boundary discontinuities have a friction angle of 37°.

These assumptions are far reaching (mainly to preserve simplicity here), and should be reviewed in as many geotechnical conditions as possible in order to evaluate their validity.

In order to make a quick assessment, the geotechnical engineer should measure the position of the closest tensile fracture behind the slope crest, and then measure the position of the tensile fracture furthest from the slope crest. The difference between these is the active block width (see Figure 10). Then, knowing the height of the slope, one must ask the question: is $h > w / 2$? (See Figure 18 for a definition of these variables). If so, then it is worth going ahead with the simple assessment. The active and passive block volumes per metre of slope are given by (see Figure 18 for the meaning of the variables):

$$V_a = wh - \frac{w^2}{4} m^3/m \text{ of slope}$$

for the active block, and

$$V_p = \frac{1}{2}h^2 \sec(q) + ch + \frac{1}{4}w^2 \;\; m^3/m \text{ of slope}$$

for the passive block, when assuming the slope geometry given in Figure 18.

In assessing the potential for failure using these volumetric equations, let $h = aw$, and $c = bw$.

Then

$$V_a = aw^2 - w^2/4 \;\; m^3/m \text{ of slope}$$

and

$$V_p = \frac{a^2w^2}{2\tan\theta} + abw^2 + w^2/4 \;\; m^3/m \text{ of slope},$$

and the stabilizing force is:

$$F_s = \left(\frac{a^2w^2}{2\tan\theta} + abw^2 + w^2/4\right)\rho g\mu \sin\theta \;\; N/m \text{ of slope},$$

while the upsetting force is:

$$F_u = \left(aw^2 - w^2/4\right)\rho g\mu \cos\theta \;\; N/m \text{ of slope}.$$

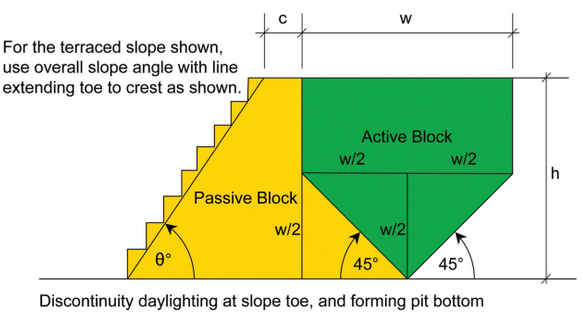

Figure 18—generalized active and passive block geometry for simplified field analysis

67-85:Template Journal 6/5/09 11:06 AM Page 319

Engineering application of thrust block analysis in slope stability problems

Defining the slope stability in terms of a factor of safety:

$$FoS = \frac{F_s}{F_u} = \frac{\frac{2a^2}{\tan\theta} + 4ab + 1}{4a - 1},$$

after simplification and rearrangement. This boils down to the fact that if the volume of the active block exceeds that of the passive block, then the factor of safety is less than unity. Hence, if $V_a \geq V_p$, the slope is considered unstable, and the geotechnical engineer should perform the full analysis as a matter of urgency.

It is a simple matter to draw up a series of tables using a spreadsheet to determine factors of safety for variations in h, c, and θ. This simplified methodology reveals factors of safety of 1.28 for a slope angle θ of 30°, a = 1.1, and c = 0 in the case of the first slope collapse. This suggests that the geotechnical engineer should review the slope stability using the block thrust mechanism because any factor of safety less than 1.3 is considered marginal. In the case of the second failure, θ = 60°, a = 1.3, and c = 0, which gives a factor of safety of 0.59, which suggests that the slope needs urgent attention.

Detailed FOS estimation using the thrust block methodology

Based on the conjectures and assumptions described earlier, it is possible to sketch an approximate picture of the block formation and the subsequent slope failure. The Appendix contains the full analytical procedure presented by Karparov[34], which should be used to predict the slope factor of safety more accurately.

The failure models, which were applied to the mine collapses, appear in Figures 4 and 5. The results from these computations, together with comparable results from accepted slope stability analyses appear in Table I, using rock parameters contained in Table II. It is apparent from the safety factor computations that circular failure is unlikely except in the case of the initial failure in the overburden in Pit A-1. Observations at the mine confirm this in both cases. Blocky failure results for Pit A-2 were essentially meaningless except for the result obtained from the ordinary method, while the initial circular failure in Pit A-1 was equally likely to manifest as blocky failure according to the Bishop[14], Janbu[16] and Ordinary Methods[13], while the

Table I

Slope collapse safety factors, calculated for the failures presented in Figures 4 and 5 (after Karparov[34])

Analytical technique	Thrust failure mechanism	Ordinary	Bishop	Janbu	Morgenstern-Price	
					Moment	Force
Pit A-2						
Circular failure	-	2.434	2.649	2.354	2.572	2.569
Blocky failure	-	1.198	0.157	0.152	0.113	0.144
Upper contact (spoil)	1.375	-	-	-	-	-
Lower contact (spoil)	0.777	-	-	-	-	-
Upper con. (no spoil)	1.287	-	-	-	-	-
Lower con. (no spoil)	0.794	-	-	-	-	-
Pit A-1 Initial failure						
Circular failure	-	0.709	0.729	0.708	0.722	0.716
Blocky failure	-	0.738	0.733	0.715	0.103	0.104
Pit A-1 major collapse						
Circular failure	-	1.506	1.516	1.507	1.513	1.509
Blocky failure	-	4.718	4.619	4.329	4.870	4.870
Upper contact	1.224	-	-	-	-	-
Bottom contact	0.908	-	-	-	-	-

Table II

Rock parameters used in the factor of safety calculations (after Karparov[34])

Rock properties	Sandy overburden	Sandstone	Shale (normal to bedding)	Shale (parallel to bedding)
1	2	3	4	5
Density, kg/m3	1900	2600	2700	-
Shear modulus, GPa	1.6	5.2	2.3	-
Bulk modulus, GPa	2.6	5.9	4.5	-
Tensile strength, MPa	1	5.5	3.5	1
Cohesion, kPa	40	700	400	100
Friction angle, deg.	32	22	14	8
Layer thickness*, m	20	12	8	-

*Average layer thickness

67-85:Template Journal 6/5/09 11:06 AM Page 320

Morgenstern-Price[17] method produced meaningless results. As far as the major collapse was concerned in Pit A-1, all accepted methods indicated that circular failure was unlikely, and that blocky failure was extremely unlikely. Table 1 shows that in both cases, the thrust failure mechanism has a reasonable chance of occurring, while all the other methods yielded less consistent results.

Discussion and conclusions

The thrust mechanism failure potential was applied to the two major collapses assuming a slip surface on the upper shale contact, and a second failure surface on the lower shale contact with the middle coal seam. The purpose of this was to test the potential of the mechanism to differentiate between potential collapse on one failure surface and another. In both cases, no failure was predicted for the upper shale contact, while collapse was predicted for the lower shale contact. This is in line with the observations at the mine. Interestingly, the spoil pile in Pit A-2 had a slight stabilizing effect, although this was insufficient to prevent collapse.

The thrust failure mechanism appears to be promising as a new slope stability analysis technique because it can potentially be applied to a wide variety of geotechnical conditions. It has been tested in two well-documented cases, and has been shown to be successful, in contrast to the other inappropriately applied methods. This does not mean that the method is infallible—proof of success is acceptable only if the proposed technique can be shown to work in nearly every possible case where the block thrust mechanism is suspected, and where all failures to work can be shown to be the result of inappropriate application of the method.

The authors have not been able to publish more failure cases than have been analysed using this method, but have decided to publish this paper in order to make this method known in the hope that other workers in the field will be willing to help test its potential on pit failures they have observed, and which conventional methods have failed to predict. The biggest stumbling block to obtaining data on slope failure cases resides with the mines: usually a slope failure is an expensive and embarrassing phenomenon that mine management prefers to hide from public view. This explains the anonymity of the two cases discussed above. However, the literature review clearly shows that many slope failures are unpredictable using conventional methods, and this, not the incompetence of geotechnical engineers or mine management, has probably led to the design of potentially unstable slopes. The authors therefore appeal to the industry for access to unexplained slope failures as soon as they have occurred, so that this methodology has a chance of being tested more widely.

The proposed thrust failure analysis is a versatile method for slope stability assessment in complex geotechnical conditions in cases where the block thrust mechanism is suspected. The complexity of the analysis should loosely reflect the complexity of the geotechnical conditions in which potential failure may take place. It will not be infallible as an approach because of subjectivity on the part of the engineer involved. Successful application will depend on a careful balance between simplicity, in which the block thrust model is analytically tractable, and complexity, where the essential features of the geotechnical conditions that affect potential failure potential are included.

Typically, mines are situated in more or less uniform mining environments, which are the result of a combination of the palæo-geological conditions that existed at the time of the formation of the orebody, and the subsequent geological history of the area up to the time of mining. The geological history refers to the changing geological conditions that the orebody may be subjected to after its formation, for example, periods of crustal stress intensification and stress relaxation; erosion of overlying rock and deposition of new sediments; fault, fold, and joint formation; chemical alteration by weathering or regional metamorphism; and intrusion by dykes and sills. All orebodies will be subjected to a combination of some or all of the above processes once or more during their geological history and these will result in a mining environment unique to the orebody.

Within the mining environment there will be one or more geotechnical areas, for example faulted ground and unfaulted ground. The block thrust failure mechanism may then only be possible in faulted ground for example, while other slope stability problems may be extant in the unfaulted ground. It will be the duty of the engineer and geologist to identify these conditions, determine the potential for slope collapse, and then propose appropriate precautions where necessary.

The following conclusions can be drawn:

- The analysis technique takes into account the most likely virgin and resultant stress state of the slope profile, and their potential effect on slope collapse
- With the aid of this method a more realistic slope stability safety factor and appropriate general slope angle design are possible
- The methodology includes the effect of pore-water pressure on potential collapse
- The method deserves further attention, but the authors have not been able to obtain data on more that the above-described failures
- A simple quick assessment method generalizes a slope and block geometry, and then applies a simple criterion to make a preliminary in-pit slope stability assessment
- This paper is published in the hope that the block thrust mechanism will receive wider attention and application in the mining industry, both in South Africa and abroad.

The authors consider this paper a contribution as it provides engineers with another tool to assess slope stability in circumstances where the accepted methods are known to fail. The authors recommend that this method should be applied to as many case studies from the worldwide mining industry as possible, where sufficient detail of each individual failure and the geological conditions are available. Secondly, fracture development in rock will receive a boost from an investigation into Riedel's work[37], and this should be applied to predicting the potential for the growth of shear fractures, and the resulting potential instability, in all geotechnical conditions.

67-85:Template Journal 6/5/09 11:06 AM Page 321

References

1. Hoek, E. and Bray, J.W. *Rock slope Engineering*. The Institute of Mining and Metallurgy, London, 1981.
2. CANMET. *Pit Slope Manual*, Mining research Laboratories, CANMET, Canada 1997.
3. Harries, N. Personal communication at the International Symposium on Slope Stability, Cape Town, 4–7 March 2006.
4. Sturman, J.M. Influence of slope stability on economics of opencast coal mining in the east and north midlands of England. *Second International Surface Mining and Quarrying Symposium*, 4–6 Oct. 1983, Bristol, UK, 1984. pp. 217–224.
5. Singh, T.N. and Singh, D.P. Assessing stability of voids in multi seam opencast mining. *Colliery Guardian*, July 1992, pp. 159–164.
6. Malgot, J., Baliak, F., and Mahr ,T. Prediction of the influence of underground coal mining on slope stability in the Vtacnik mountains. *Bulletin of the International Association of Engineering Geology*, vol. 33, 1986. pp. 57–65.
7. Boyd, G.L. Geomechanics research applied to open strip coal mining in Australia. *Second International Surface Mining and Quarrying Symposium*, 4–6 Oct. 1983, Bristol, UK, 1983. pp. 193–204.
8. Skempton, A.W. and Hutchinson, J.N. Stability of natural slopes and embankment foundations, State-of-the-art report, *Proc 7th Int Conf SMFE*, Mexico City, 2, 1969. pp. 294–335.
9. Stead, D. and Scoble, M.J. Rock slope stability assessment in British surface coal mines. *Second International Surface Mining and Quarrying Symposium*, 4–6 Oct. 1983, Bristol, UK, 1983. pp. 205–216.
10. Anderson, M.G. and Richards, K.S. *Slope stability—geotechnical engineering and geomorphology*. Reprinted, John Wiley & Sons. 1992.
11. Bromhead, E.N. *The Stability of Slopes*. Surrey University Press, Chapman and Hall, New York, 1992. pp. 109–165.
12. Wright, S.K., Kulhawy, F.H., and Duncan, J.M. Accuracy of equilibrium slope stability analysis. *J. of the Soil Mech. and Found. Div*., ASCE, vol. 99, no. SM10, 1973. pp. 783–791.
13. Fellenius, W. Calculation of the stability of earth dams. Trans. *2nd Congr. on Large Dams, Washington*, vol. 4, 1936. pp. 445–459.
14. Bishop, A.W. The use of the clip circle in the stability analysis of earth slopes. *Geotechnique*, vol. 5, 1955. pp. 7–17.
15. Lowe J. and Karafiath L. Stability of earth dams upon draw down. *Proc. 1st Pan-Am. Conf. Soil Mech. Found. Eng*., Mexico, vol. 2, 1960. pp. 537–560.
16. Janbu, N. Stability analysis of slopes with dimensionless parameters. *Harvard University Soil Mech*. Series, no. 46. 1957.
17. Morgenstern, N.R. and Price, V.A. The analysis of the stability of general slip surfaces. *Geotechnique*, vol. 15, 1967. pp. 79–93.
18. Spencer, E.E. A method of the analysis of the stability of embankments assuming parallel inter-slice forces. *Geotechnique*, vol. 17, 1967. pp. 11–26.
19. Turnbull, W.J. and Hvorslev, M.L. Special problems in slope stability, ASCE, *J. Soil Mech. Fdnt. Div*., 93, (SM4), 1967. pp. 499–528.
20. Whitman, R.V. and Bailey, W.A. Use of computers for slope stability analysis, ASCE, *J. Soil Mech. Fdnt. Div*., 93, (SM4), 1967. pp. 475–498.
21. SRK. Failure analysis of the North Pit Failure, Colliery A-1. unpublished internal mine report. 1995.
22. Canady, I.I. Personal communication. Head of failure slope profiling team, 1999. 2006.
23. Mattushek, M. Personal Communication. Divisional Geologist, New Vaal Colliery, South Africa. 2005.
24. Cairncross, B. Paleodepositional environments and tectono-sedimentary controls of the postglacial Permian coals, Karoo Basin, South Africa. *International Journal of Coal Geology*, vol. 12, 1989. pp. 365–380.
25. Snyman C.P., and Barclay J. The coalification of South African Coal. *International Journal of Coal Geology*, vol. 13, 1989. pp. 375–390.
26. Voight, B. Beziehung zwischen grossen horizontalen Spannungen im Gebirge und der Tektonik und der Abtragung. *1st Congress Int. Soc. Rock Mech*., Lisbon, 1966, vol. 2, pp. 51–56.
27. Gay, N.C. *In situ* stress measurements in Southern Africa, *Tectonophysics*, vol. 29 1975. pp. 447–459.
28. Gay, N.C. The state of stress in a large dyke on E.R.P.M., Boksburg, South Africa. *Int. J. Rock Mech. Min. Sci. & Geomech. Abstr*., vol. 16, 1979. pp. 179–185.
29. Stacey, T.R. and Wesseloo, J. *In situ* stresses in mining areas in South Africa. *Jour. S. Afr. Inst. Min. and Metall.* vol. 98, no. 7, 1998. pp. 365–368.
30. Sellers, E.J., Coetzer, S.J., and Kamstra, R. *Understanding and Determining the Variability of the Primitive Stress Environment*. SIMRAC Research Project GAP707, Department of Minerals and Energy, Pretoria, March 2002.
31. Van der Merwe, J.N. Personal communication, Department of Mining Engineering, University of Pretoria. 2002a.
32. Van der Merwe, J.N. Horizontal stress: The root of all evil?, *Proc. 19th Conf. on Ground Control in Mining*, Teheran, Iran. 2002b.
33. Hoek, E. and Brown, E.T. *Underground Excavations in Rock*. The Institution of Mining and Metallurgy, London, 1980. p. 100.
34. Karparov, KN. Slope Stability Analysis in Complex Geotechnical Conditions—Thrust Failure Mechanism. PhD Thesis submitted for examination to the University of Pretoria, Pretoria, South Africa, August 2006.
35. Itasca Consulting Group. *FLAC2D: Fast Lagrangian Analysis of Continua*. Minneapolis, Minnesota, USA. 1999.
36. Barton, N.R. A Model Study of the Behavior of Excavated Slopes. Ph.D. Thesis, University of London, Imperial College of Science and Technology. 1971.
37. Riedel, W. Zur mechanik geologisher brucherscheinungen. Zentralblatt fur Mineralogie, *Geologie und Paleontologie B*, (Abhandlung). 1929. p. 354–368.
38. Lade, P.V., Cole, D.A., and Cummings, D. Multiple failure surfaces over dip-slip faults. *Journal of Geotechnical Engineering*, vol. 110, no. 5, May 1984, 1984. pp. 616–627.
39. Sylvester, A.G. Strike-slip faults. *Bulletin of the Geological Society of America*, vol. 100, 1988. pp. 1666–1703.
40. Vermeer, P.A. and De Borst, R. Non-associated Plasticity for Soil, Concrete and Rock, *Heron*, vol. 29, no. 3, Delft University of Technology, Delft, The Netherlands. 1984.
41. Ortlepp, W.D. *Rock Fracture and Rockbursts: an illustrative study*. Monograph Series M9, South African Institute of Mining and Metallurgy, Johannesburg. 1997.
42. Gammond, J.F. Displacement features associated with fault zones: a comparison between observed examples and experimental models. *Journal of Structural Geology*, vol. 5, 1983. pp. 33–45.
43. Jaeger, J.C. and Cook, N.G.W. *Fundamentals of Rock Mechanics*, 3rd Ed. New York, Chapman and Hall. 1979.
44. Kovari, K. and Fritz, P. Special contribution: Slope stability with plane, wedge and polygonal sliding surfaces. *Symposium on Rock Mechanics Related to Dam Foundations,* Rio de Janeiro. 1978.
45. Baer, G. Mechanisms of dike propagation in layered rocks and in massive porous sedimentary rocks. *Journal of Geophysical Research 96*, vol. 11, 1991. 911–11, 929.
46. Narr, W. and Suppe, J. Joint spacing in sedimentary rocks. *Journal of Structural Geology*, vol. 13, 1991. pp. 1037–1048.
47. Gross, M., Fischer, M., Engelder, T., and Greenfield, R. Factors controlling joint spacing in interbedded sedimentary rocks; integrating numerical models with field observations from the Monterey Formation, USA. Ameen, M.S. (ed.). *Fractography*. Geological Society Special Publication, Geological Society, London, 1995. pp. 215–233.
48. Becker, A. and Gross, M. About the Dugdale crack under mixed mode loading. *Int J Fracture,* 37. 1988.
49. Ji, S. and Saruwatari, K. A revised model for the relationship between joint spacing and layer thickness. *Journal of Structural Geology*, vol. 20, 1998. pp. 1495–1508.
50. Helgeson, D.E. and Aydin, A. Characteristics of joint propagation across layer interfaces in sedimentary rocks. *Journal of Structural Geology*, vol. 13, 1991. pp. 897–991.
51. Tsang, Y.W. The effect of tortuosity on fluid flow through a single fracture. *Water Resources Research*, vol. 20, 1984. pp. 1209–1215.
52. Itasca Consulting Group. *FLAC2D. Fast Lagrangian Analysis of Continua*, 1999.
53. Hoek, E. Slope stability analysis. Lecture at Santiago Technical University, Chapter 7—A: Slope stability problems in Hong Kong, 1986. pp. 92–104.

67-85:Template Journal 6/18/09 2:58 PM Page 322

Engineering application of thrust block analysis in slope stability problems

Appendix A

Method of thrust failure mechanism analysis for slope stability in complex geotechnical conditions

Introduction

The proposed failure mechanism is related to the polygonal failure surfaces theory by Kovari and Fritz[44], Boyd's[7] observations (see Figure 1), and the work of Stead and Scoble[9]. Accepted literature shows that sliding usually takes place on surfaces that can be modelled by concave-up polygonally shaped surfaces. For such cases, Janbu[16], and Morgenstern and Price[17] have suggested practical methods of computation, according to which the unstable earth- or rock-mass is divided up into vertical strips or slices.

The Kovari and Fritz[44] polygonal failure surfaces theory is based on certain assumptions about the distribution and inclination of the internal contact forces, as well as the hypothesis of limit equilibrium. Their method is based upon the physical requirement that sliding on a polygonal surface is only possible kinematically if a sufficient number of internal shear surfaces can develop. For the sake of simplification, only continuous shear surfaces starting from the intersection lines of the polygon-sliding surface are assumed. Thus, as shown in Figure A.1, the slide of a mass on three surfaces must be accompanied by at least two internal shear surfaces. For n external sliding surfaces (n-1) such interfaces are required.

This approach complicates the theory and makes it kinematically more difficult to justify. The thrust block mechanism resolves this dilemma by retaining the multiplanar failure surface, and substituting the two rear-most blocks in Figure A.1 with a single active block. The passive block is equivalent to the front block in Figure A.1, albeit with a different geometry.

The Kovari and Fritz[44] method rests upon the following basic assumptions:

- The blocks comprising the rock mass are each considered to be rigid
- The directions of the internal shear surfaces are known
- On the internal and external sliding surfaces (at the condition of limit equilibrium), the Mohr-Coulomb failure criterion applies, and no tensile strength is permitted. The strength parameters may be allocated different values on each sliding surface.

The directions of the internal shear surfaces are chosen from case to case based on a careful investigation of the structure of the potentially sliding mass. However, for highly jointed rock, the directions of the internal slip surfaces are found by the condition of a minimum safety factor for the system. The Kovari and Fritz[44] method does not take into account the existence of complex geotechnical structure within the slope. It also ignores the formation of a tensile fracture behind the slope crest, which is a common feature in competent rock slopes. In their method, the internal failure surfaces are determined by careful field observation, which has an element of subjectivity introduced by observer experience, but it appears that the multi-planar nature of the shear surface is well established.

The proposed thrust failure mechanism therefore simplifies Kovari and Fritz's[44] method by using only three failure surfaces because the investigated slope profile is divided into two blocks, namely passive and active blocks (see Figure 10 in main text). The proposed method also takes into account the tensile fracture behind the slope crest.

Formation of tensile fractures

Tensile crack formation behind the slope crest is widely observed and reasonably well understood. In a series of very detailed model studies on slope failures, Barton (1971) found that the tension crack behind the slope crest was generated by small movements within the rock mass, and that it appeared after slope excavation. Although these individual movements were very small, their cumulative effect was a significant displacement of the slope surface towards the pit—sufficient to cause separation of material behind the slope crest and to form tension cracks. Using a FLAC[52] model, Karparov[34] estimated the position of the tensile zone in the slope, shown in Figure A.2. This line then defines the vertical extent of the tension fractures, which are shown in blue in Figure A.2.

Formation of shear fractures at base of active block

Fracture development in rock is complex and remains poorly understood. In layered sedimentary rocks, opening-mode fractures have been observed to abut against bedding contacts (Baer[45], Narr and Suppe[46], Gross *et al.*[47], Becker and Gross[48], and Ji and Saruwatari[49]), cross through contacts

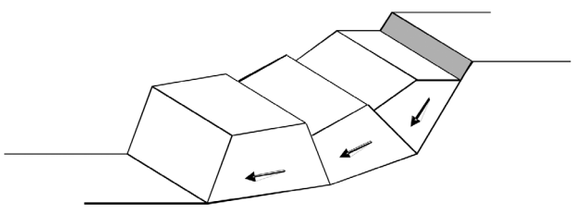

Figure A.1—Kinematics of a slope failure for a polygonal sliding surface (after Kovari and Fritz[44])

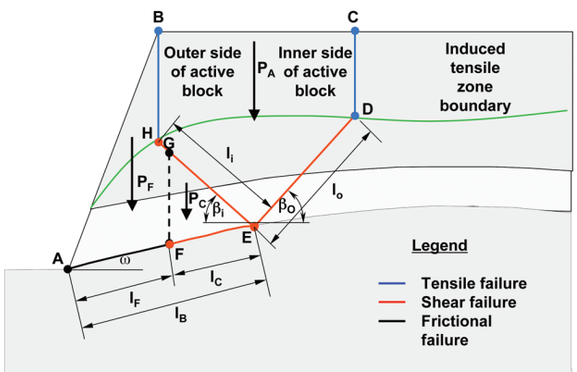

Figure A.2—Formation of active block bounded by tensile and shear fractures

67-85:Template Journal 6/5/09 11:06 AM Page 323

(Becker and Gross[48]), and jog or step-over at bedding contacts (Helgeson and Aydin[50]). Fracture termination at frequent bedding contacts can produce highly tortuous fracture paths in sediments (Tsang[51]). By contrast, fractures that propagate straight through bedding provide well-connected pathways. A potential intermediate case is a fracture that jogs or steps over a few centimetres at bedding contacts (Helgeson and Aydin[50]). Although these three types of fracture intersection with bedding are easily recognized in the field, the mechanisms that control the degree of fracture offsetting across bedding surfaces are not yet well understood. Insight into controlling mechanisms and parameters could aid the prediction of subsurface fracture propagation.

In solid rock material where jointing and other structures are insignificant, shear failure is a complex process resulting in complex fracture structures. In broken rock masses opportunistic shear may take place along pre-existing fractures, with the result that the shear fractures are likely to be simpler. A common terminology for brittle shear fractures in rock is introduced below (adapted from Riedel[37], Sylvester[39], and Vermeer and de Borst[40]) and shown in Figures 8 and 9 in the main text. Riedel's[37] paper is not available, and his work is completely unknown in solid mechanics, while it is widely referenced in structural geology. The reproductions of his interpretations in Sylvester[39] and McKinnon and De la Barra[52] are probably misleading because there is no mechanistic description of how the various fractures develop. Riedel's work should be revisited from a solid mechanics point of view, because it provides a good starting point for the interpretation, from a stress and deformation point of view, of small and large faults in rock masses.

The best location in the slope for shear fracture formation is just below the modelled horizontal tensile zone, where the horizontal stresses will be small. There is a mechanistic reason for this because this point has the maximum isolated block weight above it (the block is assumed to be defined by two or more tensile fractures behind the slope crest) and this should be a favourable point for the origin of shearing, where the horizontal stresses are low. The shearing fractures are also assumed to have the complexity of shearing seen in all geological materials, i.e. along faults, in mines, and in the laboratory. Since Riedel[37] presented his shearing model, it has been widely accepted and has repeatedly been demonstrated to be a reliable guide for the interpretation of shear along all types of geological features. Karparov's[34] work contains more detail on Riedel Fractures.

The purpose of presenting all this detail is to recognize that the formation of shear zones in the slope is likely to be complex, just as they are in any geological material. However, Riedel's[37] observation that the shear fracture structure is complex, contrasts with the simple observation that the shear zone orientation is most likely to lie parallel with the direction of the largest shear stress in the slope, which is approximately 45° from the horizontal, given the FLAC model results[34].

Linking the active block to pit slope

Karparov[34] presents a more complex picture, but it can be assumed that the surface AFE linking the slope toe and the active block base in Figure A.2 is frictional. The surface may have been cohesive, and Karparov[34] undertook microscopic studies to demonstrate how the cohesive bonds on this surface could have been broken. It was concluded that this study did not produce indisputable results, and that more research was needed. Anyway, the surface must eventually become frictional, because both failures investigated showed this to be the case. Once all the tensile and shear fractures have linked together to form the block geometry shown in Figure A.2, slope failure is inevitable, if the active block is sufficiently large to thrust the passive block into the pit.

Analysis of trust failure mechanism

It is also important to recognize that this analysis considers force equilibrium, but in deformable block structures. It therefore assumes that all forces should pass through the block centroids, because this is necessary to explain the irrotational nature of the failures. In other words, moment equilibrium is not considered in this model because observations of the failures at the mine did not reveal any significant rotational motion in the failures.

Figure A.2 indicates the failure types and lengths used for the purpose of the slope stability calculations. Symbols used in the analysis are as follows:

- P_A, P_F, P_C are the load of the active block and the frictional and cohesive zones of the passive block respectively
- $\bar{c}_I$, $\bar{c}_O$ are the cohesions of the inner and outer side of the active block respectively
- l_I, l_O are the shear failure lengths of the inner and outer side of the active block respectively
- l_F, l_C are the lengths of the frictional strength zones and the cohesive strength zones of the passive block failure surface respectively
- l_B is the length of the passive block failure surface and is equal to the sum of the lengths of frictional strength and cohesive strength zones ($l_B = l_F + l_C$)
- β_I, β_O are the shear failure surface angles at the inner and outer sides of the active block respectively (assumed to be 45°)
- R_P is the reaction of the passive block applied to the active block
- f_{avI},f_{avO} are the average internal friction angles along the shear failure surfaces at the inner and outer side of the active block respectively
- w is the dip angle of the strata.

The average friction angle along each surface in a multi-layered medium can be expressed as the weighted average:

$$\phi_{ave} = \frac{\sum_{i=1}^{n} m_i \phi_i}{\sum_{i=1}^{n} m_i} \qquad [A.2]$$

where m_i is the layer thickness of the ith layer and f_i is the frictional angle of the ith layer.

Like the friction above, the average cohesion is also calculated along the shear failure surfaces of the active block sides as the weighted average:

67-85:Template Journal 6/5/09 11:06 AM Page 324

$$C_{ave} = \frac{\sum_{i=1}^{n} m_i C_i}{\sum_{i=1}^{n} m_i} \quad [A.3]$$

where m_i is the failure surface length in the ith layer and C_i is the cohesion of the layer intersected by the active block shear failure surface.

The active block weight for unit thickness is calculated as:

$$P_A = g \sum_{i=1}^{n} \rho_i A_i \quad [A.4]$$

where A_i is the layer volume in the active block profile, ρ_i is the layer density, and g is the acceleration due to gravity.

The active block is constructed in the following way, using the tensile fracture positions measured on the slope crest:

- Draw two tensile fractures vertically downwards from surface at the positions they were seen on surface
- Find the midpoint of a horizontal line joining the two fractures, and project this vertically downward to intersect the frictional surface line (the surface the passive block will slide on)
- Project two shear failure surfaces up at angles of 45° to the horizontal from the intersection point on the frictional surface until each intersects their respective vertical tensile fractures.

The active block is now defined (see Figure A.2, or Figure 10 in the main text). This construction is not intended to represent the sequence of development of these fractures as there is still insufficient evidence to determine exactly how the failure surfaces do grow within the slope, or even if the grow sufficiently to link up. Once all these fractures are developed and connected, the formation of the active block is complete.

As was mentioned earlier, we may have two zones along th failure surface at the passive block base, namely the frictional and cohesive zones. These two zones have different shear strengths, which have to be taken into account when the resistance force developed by the passive block is computed. The passive block weight calculation is the same as for the active block.

Resisting forces at the base of the passive block are formed by the frictional strength along the failure surface due to the block weight and the cohesive and frictional strength of that portion of the contact surface that has not yet yielded in shear. Driving forces are formed by the tangential component of the weight along the same surface. Hence, these forces can be expressed as:

$$P_F^N = P_F \cos\varpi \quad [A.5a]$$

$$P_F^{dr} = P_F^T = P_F \sin\varpi \quad [A.5b]$$

where ϖ is an average inclination angle of the failure surface, P_F is the passive block load above frictional zone, P_F^N and P_F^T are the normal and tangential components respectively. The resisting force along the frictional zone will have the form:

$$P_F^{res} = P_F^N \tan\phi_E = P_F \cos\varpi \tan\phi_E \quad [A.6]$$

where ϕ_E is the frictional angle along the bedding.

Similar to the frictional zone, normal and tangential load components in the cohesive zone of the passive block can be calculated with Equation [A.7]. Then the resisting and tangential forces to the failure surface will have the form:

$$P_C^{res} = c_B l_B + P_C^N \tan\phi_B = c_B l_B + P_C \cos\varpi \tan\phi_E \quad [A.7a]$$

and

$$P_C^{dr} = P_C \sin\varpi_C \quad [A.7b]$$

respectively.

Figure A.2 shows that the rock mass rests on two potential failure surfaces: the frictional surface AFE, and the active block inner shear failure surface ED. This is very similar to the Kovari and Fritz[44] geometry discussed earlier. Thrust block failure is possible only if slip surface EG in Figure A.2 is developed. This has forces acting on it as shown in Figure A.3.

From Figure A.3 we can write

$$\overline{T}_{\max} = \overline{N} \tan\phi + cl \quad [A.8]$$

If we take into account the definition for safety factor

$$FoS = \left| \frac{\text{maximum shear resistance}}{\text{applied shear stress}} \right| \quad [A.9]$$

Then we can write

$$FoS = \frac{\overline{S}_{\max}}{S} = \frac{\overline{N} \tan\phi}{\overline{T}} + \frac{cl}{\overline{T}} \quad [A.10]$$

From Figure A.3 and Equation [A.10] we have

$$\tan\delta = \frac{\overline{T}}{\overline{N}} = \frac{1}{FoS}\left(\tan\phi + \frac{cl}{\overline{N}}\right) \quad [A.11]$$

and

$$\overline{N} = R\cos\delta \quad [A.12]$$

If we combine Equations [A.11] and [A.12] and accept FOS = 1, which means that the internal slip surface is at the point of slipping, then we will have

$$\tan\delta = \tan\phi + \frac{cl}{R\cos\delta} \quad [A.13]$$

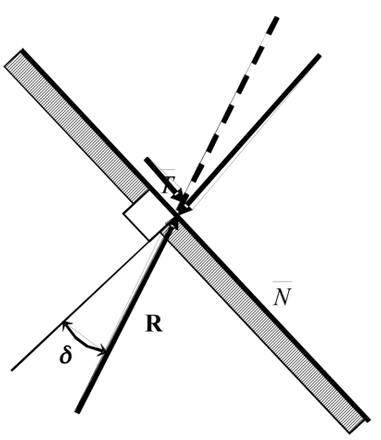

Figure A.3—Detail of internal 45° shear surface

67-85:Template Journal 6/5/09 11:06 AM Page 325

The angle of internal friction in Equation [A.13] has to satisfy the condition in Equation [A.14] if it is to have a real solution:

$$\phi \geq \sec^{-1}\left(\frac{cl}{R}\right) \qquad [A.14]$$

From Equation [A.14] we can see that under worst-case conditions, $\phi = 0°$ if $\frac{cl}{R} = \infty$, which is possible only if $R = 0$, and both $c \neq 0$ and $l \neq 0$. In the case of $l = 0$, we should have a tensile fracture from the surface to the failure surface. Kovari and Fritz[44] accepted the worst-case scenario in their polygonal model, which gives the angle of reaction forces as equal to the angle of internal friction ($\delta = \phi$).

The following equations can be applied for the active block load distribution along the two shear failure surfaces that form the wedge structure:

$$P_{AO} = \frac{P_A}{2}\left(1 + \sin\varpi_A\right) \qquad [A.15]$$

and

$$P_{AI} = \frac{P_A}{2}\left(1 + \sin\varpi_A\right) \qquad [A.16]$$

for the outer and inner shear failure surfaces respectively (see Figure A.2 for a definition of 'outer' and 'inner'), where PA is the weight of the active block and ϖ_A is the layer inclination angle at the block wedge.

Figure A.4 shows the same slope profile as shown in Figure A.2, with points defining the block boundaries. Let us first calculate the pore-water pressure along the line CD in Figure A.4. The earlier calculated induced vertical tensile fracture depth (z) and a phreatic surface, (z_{WT}), above the tensile fracture depth are indicated.

Therefore, the pore-water pressure at point D in Figure A.4 is equal to:

$$\sigma_w^D = \gamma_w z_{WT} \qquad [A.17]$$

where γ_w is the unit weight of water and z_{WT} is the surface tensile fracture depth below the phreatic surface. The total force acting along the surface vertical tensile fracture at the active block outer side is equal to

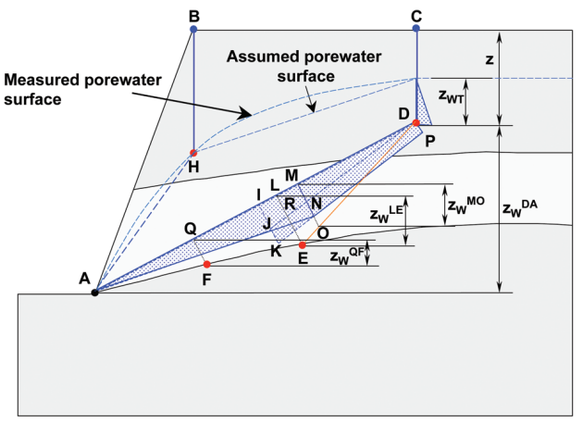

Figure A.4—Plot of pore-water pressures in the slope

$$V_w^{CD} = \frac{\gamma_w z_{WT}^2}{2} \qquad [A.18]$$

Let us calculate the pore-water pressure along the line DE. As a first step, let us define pore-water pressure along the line DA. For this purpose, we assume zero pore-water pressure at point D. We also have zero pressure at point A at the slope toe position, if there is no water flowing out of the slope. Hence, we assume that, in the middle of the span between these two points (point I), we will have the highest pore-water pressure value that will be equal to:

$$\sigma_w^I = \frac{\gamma_w z_w^{DA}}{2} \qquad [A.19]$$

where z_W^{DA} is the difference between depths of points D and A. Now we cam draw a stress diagram (ADJ) between the points A and D.

From Equation [A.17], we have pore-water pressure at point D. So let us draw the line DP, equal to the pore-water pressure at point D normal to the line AD and add the same stress magnitude at point I as adding stress JK. Now our stress diagram takes a new form (AJKPD), which is unrealistic because of the step AJK. As the point I is in the middle of AD, then half of the stress JK can be added to the portion AI and the other half to the portion ID. Hence, we have a new stress equal to

$$\sigma_w^I = 0.5\gamma_w\left(z_w^{DA} + z_{wI}\right) \qquad [A.20]$$

which is equal to the line MN in our stress diagram. Then let us move our stress magnitude MN toward point D until it intersects the stress line KP. This position is shown in Figure A.4. Now we have a new stress diagram (ANPD), which presents pore-water pressure distribution along the line AD.

Let us now calculate the pore-water pressure at point E. For this reason, let us make its orthogonal projection to the line AD, which is point L, which has pressure with the magnitude LR. Therefore, the pore pressure at point E will have the magnitude

$$\sigma_w^E = \sigma_w^L + \gamma_w z_w^{LE} \qquad [A.21]$$

where z_ω^{LE} is the depth difference between the points L and E. This pressure is realistic because point E is slightly deeper than point L.

To find the point where we have maximum pore-water pressure along the outer shear failure surface we define point O, whose orthogonal projection to the line AD is point M. With a high degree of approximation, we can say that the pore-water pressure at point O is equal to

$$\sigma_w^O = \sigma_w^M + \gamma_w z_w^{MO}. \qquad [A.22]$$

It is now easy to construct a pore-water pressure diagram along the line of the inner shear failure surface (HE) because we have calculated the pore-water pressure at point E (Equation [A.21]) and have assumed zero water pressure at point H. This assumption is based on the close point position to the two free surfaces AB and BC.

Pore-water pressure at point F follows the same order as for point E (Equations [A.21] and [A.22]):

$$\sigma_w^F = \sigma_w^Q + \gamma_w z_w^{QF} \qquad [A.23]$$

where σ_W^Q is the pore-water pressure magnitude at point Q and z_W^{QF} is the depth difference between the points Q and F.

67-85:Template Journal 6/5/09 11:06 AM Page 326

Now we are in position to draw the pore-water pressure diagrams along the active block failure surfaces and the passive block failure surfaces. Figure A.5 shows pore-water pressure diagrams and resultant forces V_{CD}, U_O, U_I, U_G and U_F acting along the failure surface of the vertical tensile fracture, the active block outer and inner shear failure surfaces, and the cohesive and frictional lengths respectively of the passive block base. The figure also shows the calculated pore-water pressures at points D, E, O, and F respectively. According to the pore-water pressure diagrams, calculated resultant forces have the following magnitudes:

$$U_O = \frac{l_{DO}\left(\sigma_w^D + \sigma_w^O\right)}{2} + \frac{l_{EO}\left(\sigma_w^O + \sigma_w^E\right)}{2} \quad [A.24]$$

$$U_I = \frac{l_{EH}\sigma_w^E}{2} \quad [A.25]$$

$$U_C = \frac{l_{EF}\left(\sigma_w^E + \sigma_w^F\right)}{2} \quad [A.26]$$

$$U_F = \frac{l_{AF}\sigma_w^F}{2} \quad [A.27]$$

where l_{DO}, l_{EO}, l_{EH}, l_{EF}, and l_{AF} are span lengths between points DO, EO, EH, EF and AF respectively. Similar pore-water pressure analysis was undertaken by Hoek[53].

At the inner shear surface, we have the combined action of two forces. The first force takes into account the sum of driving and resisting forces (with the signs '-' and '+' respectively) along the potential failure surface of the passive block base, expressed as

$$R_P = P_F^{res} + P_C^{res} - P_F^{dr} - P_C^{dr} \quad [A.28]$$

and, secondly, the corresponding active block load.

Hence, we could have two directions of the passive block reaction force (Equation [A.28]): the first one is when the sum is negative (Figure A.6a) and the second, when the sum is positive (Figure A.6b). Acceptance of the reaction force inclination angle ($\delta = \phi$), allows us to use only cohesive strength along the inner shear failure surface. We can transfer the normal to the inner surface component of the passive block reaction force (R_P), to the outer failure surface with the corresponding inclination angle.

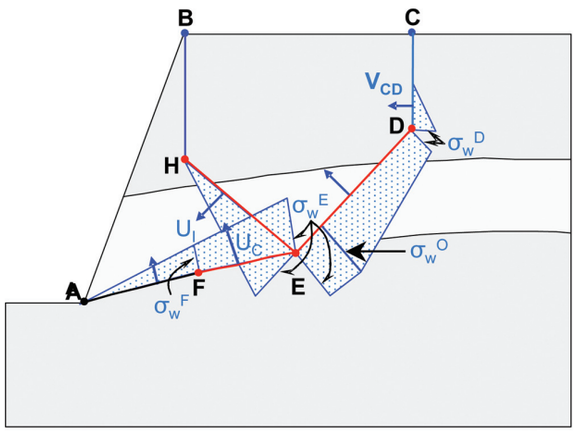

Figure A.5—Scheme for pore-water pressure calculation on the passive and active block boundaries

In the first case (Figure A.6a), the normal components on the shear surface under the passive block and the corresponding active block weight (R_P^N and P_{AI}^N) are approximately co-directional, which increases the driving forces of the active block outer shear failure surface and might lead to failure. Hence, the active block inner failure surface will have only cohesive strength.

In the second case (Figure A.6b), we have reaction force, acting opposite to the force of the active block load. Tangential (to the inner shear surface) components of the reaction force and the corresponding active block load are in opposite directions, which will decrease the total driving effect.

Using the above discussion and assumption that $\delta = \phi$ eliminates frictional resistance of the inner failure surface, we can use Equation [A.10] to define the criterion for the existence of the inner shear failure surface, which has the form:

$$\eta = \frac{cl}{P_{AI}^T - R_P^T} \quad [A.29]$$

If we take into account Equations [A.16] and [A.17] and the relationships

$$P_{AI}^T = P_{AI}\sin\beta_I \quad [A.30]$$

$$R_P^T = R_P\sin\phi_I, \quad [A.31]$$

then Equation [A.29] can be rewritten as

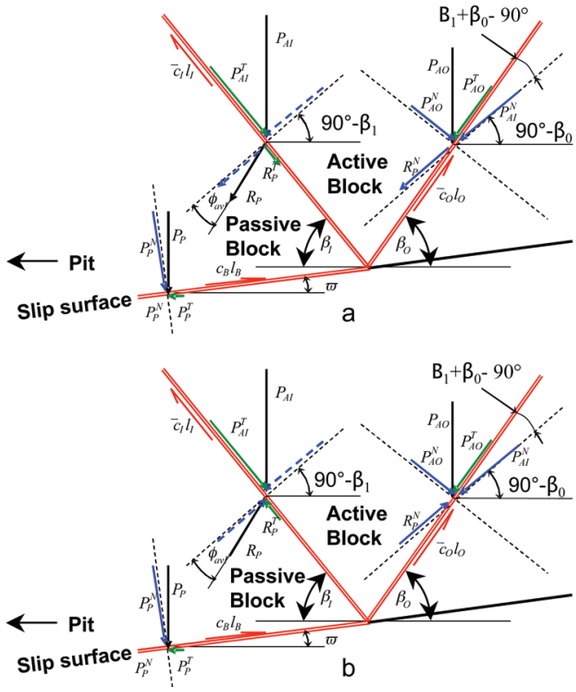

Figure A.6—Pore-water pressure diagrams on shear failure surfaces, Figure A.6a—Passive block reaction force RP acting approximately co-directional to the active block load at the inner shear failure surface, Figure A.6b—Passive block reaction force RP acting opposite to the active block load at the inner shear failure surface

67-85:Template Journal 6/5/09 11:06 AM Page 327

$$\eta = FOS_I = \frac{\bar{c}_I l_I - U_I \tan\phi_{avI}}{\frac{P_A(1+\sin\varpi_A)\sin\beta_I}{2} - R_P \sin\phi_{avI}} \quad [A.32]$$

which is a criterion for the existence of the inner shear failure surface and the surface's factor of safety.

If the shear fracture criterion (η) from Equation [A.32] is higher than 1.3, the inner shear failure surface will not form. Therefore, we will have conditions for other failure types (such as multi planar or polygonal) but not for thrust failure. If the criterion is lower than 1.3, we have to anticipate shear failure at the inner surface and, from there, blocky-type failure.

As was discussed earlier, the components normal to the inner failure surface of the corresponding active block load and the passive block reaction force are transferred to the outer shear surface. Then their combined action along the outer surface can be expressed as:

$$\bar{R} = \frac{P_A}{2}(1+\sin\varpi_A)\cos\beta_I - R_P\cos\phi_{avI} \quad [A.33]$$

Therefore, the outer shear failure surface will have a factor of safety equal to:

$$FOS_O = \frac{\bar{c}_O l_O + \left[\bar{R}\sin(\beta_I+\beta_O-90^0)+\frac{P_A}{2}(1-\sin\varpi_A)\cos\beta_O - U_O - V_{CD}\sin\beta_O\right]\tan\phi_{avO}}{\bar{R}\cos(\beta_I+\beta_O-90^0)+\frac{P_A}{2}(1-\sin\varpi_A)\sin\beta_O + V_{CD}\cos\beta_O} \quad [A.34]$$

Equation [A.34] can be further simplified as:

$$FOS_O = \frac{\bar{c}_O l_O + \left[\frac{P_A}{2}(1-\sin\varpi_A)\cos\beta_O - U_O - V_{CD}\sin\beta_O\right]\tan\phi_{avO}}{\bar{R}+\frac{P_A}{2}(1-\sin\varpi_A)\sin\beta_O + V_{CD}\cos\beta_O} \quad [A.35]$$

The basal surface safety factor presents the balance of already calculated driving and resisting forces along the contact surface in the passive block base (see Figure A.12), and has the form:

$$FOS_B = \frac{P_F\cos\varpi_F\tan\phi_B + (c_B l_C + P_C\cos\varpi_C\tan\phi_B) - (U_C+U_F)\tan\phi_B}{P_F\sin\varpi_F + P_C\sin\varpi_C} \quad [A.36]$$

where ϕ_B is the friction angle along the failure surface and v_F and v_C are the dip angles along the frictional zone and cohesive zone of the passive block base see Figure A.2).

The failure surface lengths (l_I, l_O, and l_B, Figure A.2) vary, and depend on slope angle, layer inclination, layer thickness, and rock properties. To avoid overestimating the influence of the shortest failure surface on the entire slope stability, a weighted function of calculated safety factors should be used. Hence, we have the following weighted average equation for calculation of the entire slope stability factor of safety from the individual failure surface factors of safety and their respective lengths: ◆

$$FOS = \frac{FOS_I l_I + FOS_O l_O + FOS_B l_B}{l_I + l_O + l_B} \quad [A.37]$$